Multispectral Data-fusion and Mapping for Reconnaissance Robotics

Petra Kocmanova, Ludek Zalud, and Frantisek Burian

Abstract— the paper deals with calibration of multispectral vision systems, evaluation of the calibration and data-fusion quality in both laboratory and real-world conditions and appropriate use of these techniques for multispectral measurement in telepresence and digital 3D mapping. Two objects for multispectral calibration and fusion evaluation are described. The objects were used by our team for calibration and evaluation of advanced visual system of Orpheus-X4 robot that is taken as a demonstrator, but their use is much wider and we suggest to use them as testbed for visual and optical measurement systems of mobile robots. The multispectral fusion is used for two main purposes – real-time display to operator, e.g. through visual telepresence, or for autonomous building of spatial maps of the robot's environment. Several aspects regarding proper use of the technique for telepresence are described. Mapping system developed by our team working with multiple robots with different features is described. Several evaluation experiments related to the fusion/calibration and mapping were done and are presented in the paper. We provide the calibration software as publicly available, including source code. Our team also provides testing data for both the calibration/evaluation and mapping.

Keywords—augmented reality, multispectral fusion, robotic reconnaissance, visual control.

I. INTRODUCTION

RECONNAISSANCE mobile robotics gains importance during the last years. Visual and space measurement subsystem is typically the most important sensory equipment with most significant impact to mission success. There are many missions in today's society that may require expendable robots to perform exploration in inaccessible or dangerous environments instead of indispensable people, e.g. CBRNE (Chemical, biological, radio-logical, nuclear, explosive), counter-terrorist fight, US&R (Urban Search and Rescue), etc.

Since the missions take place in real world, the robots have to be equipped for most, if not all, possible conditions that may happen. During both military and non-military search and rescue missions the robot can meet such conditions like complete darkness, smoke, fog, rain, etc. For these conditions, visual spectrum of humans is not sufficient to provide valuable data. One of the most promising approaches for wide spectrum of situations is combination of data from visual spectrum, near infrared spectrum and far infrared spectrum. In visual spectrum (using standard tricolor cameras), the operator has the best overview of the situation, since he/she gets signal that is the most similar to what he/she knows. By using thermal imagers working in far infrared spectrum he/she can perfectly perceive even slight changes in temperatures and moreover this spectrum very well penetrates through water particles (fog, rain) plus it is almost not affected by visible light conditions. Most TOF (time-of-flight) proximity scanners and cameras work in near-infrared spectrum.

Main aim of this paper is determination of effective sensory head calibration, containing typical sensors for abovementioned situations – tricolor cameras working in visual spectrum, thermal imagers working in far infrared (FIR) and proximity camera working in near infrared (NIR), and their practical usage in telepresence and digital mapping.

Calibration plate for various spectrums and optimal image configuration is an important factor for effective calibration, so great attention is paid to it.

Various targets were designed for multispectral camera calibration. Here is a brief overview of designed targets. In [1] it was created plane test field that consists of wooden board with 57 small lamps that warm up when switched on (see Fig. 1). Test field based on a metal surface with coded and uncoded circle target points created using self-adhesive foil is described in [1] (see Fig. 2). In [2] plane with heated circle target was used for calibration of thermal imager and color camera stereo pair (see Fig. 3). In [3] a pair of thermal imagers was calibrated with checker-board pattern heated by a flood lamp (see Fig. 3).

We proposed new calibration plate and new target that are simultaneously usable for visible, near infrared and long wave infrared spectrums. This proposed plate is described below in chapter III and chapter V.

P. Kocmanova is with the LTR s.r.o., U Vodarny 2032/2a, Brno, Czech Republic, phone: +420 541141306; fax: +420 541141123; e-mail: petra.kocmanova@seznam.cz.

L. Zalud is with the LTR s.r.o., U Vodarny 2032/2a, Brno, Czech Republic and Brno University of Technology, Technicka 12, Brno, Czech Republic; e-mail: zalud@orpheus-project.cz.

F. Burian is with the LTR s.r.o., U Vodarny 2032/2a, Brno, Czech Republic; e-mail: burian@orpheus-project.cz.
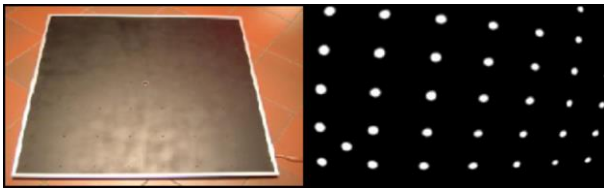
Fig. 1 plane testfield with active lamps [1]: photo (left), thermal image (right)
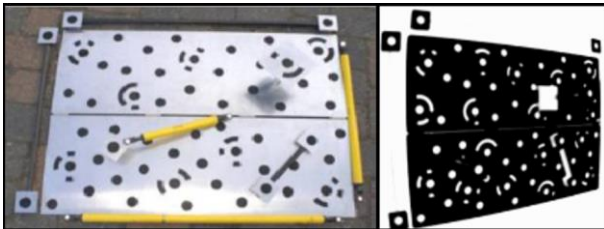

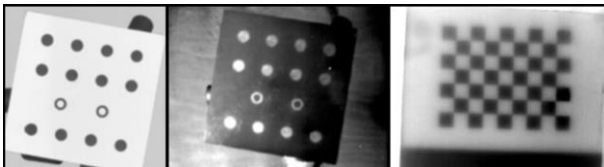Fig. 2 spatial testfield [1]: photo (left), thermal image (right)

Fig. 3 testfield seen by color (left) and infrared (center) camera [2], thermal image of calibration grid (right) [3]

Calibration of sensory head is proposed according to Zhang algorithm [4]. Zhang investigated performance of his one camera calibration algorithm with respect to number of images of the model plane. Number of images varied from 2 to 16. Error of intrinsic and extrinsic parameters decreased significantly between calibration from 2 and 3 images. Precision improves for more than images only insignificantly.

Calibration performance with respect to orientation of the model plane was also investigated in [4]. Best performance was achieved with angle 45° between calibration plane and image plane. This angle value is difficult to apply in real condition, because it decreased precision of corners extraction.

Photogrammetric software Photomodeler [5] recommends for one camera calibration using minimal 6 and optimal 8 images of calibration plate from different angles. Another recommendation is using less than 12 images for camera lenses with wide angle and high distortion. Next recommendation is making at least 2 images with roll of 90° (camera portrait, landscape orientation). Unfortunately this rotation isn't possible with proposed sensory head, because of sensory head manipulator.

Bouguet in Complete Camera Calibration Toolbox for Matlab [6] recommends to use about 20 images of planar checkerboard. 6 – 10 images should be enough for calibration in Omnidirectional Camera Calibration Toolbox for Matlab [7].

Effective image configuration for camera calibration of

sensor head of robot Orheus-X4 will be investigated in chapter IV.

In chapter IV we describe the 3D mapping system developed by our team. The system is made to incorporate multispectral data and is able to work with multiple sources of data from different sources, i.e. different robots with different features, e.g. sensors. Special attention is paid to data exchange among more robots including lossless compression due to necessity of wireless transfer of the data during real missions.

II. HARDWARE

Our main concern is to make the systems practically usable. So we develop and test them on reconnaissance robotic system CASSANDRA that is being developed by our team.

Although the CASSANDRA robotic system is rather complex and contains several interesting robots, only the Orpheus-X4 is important for the purposes of this paper. CASSANDRA robots and the system itself are described in detail in [16].

Fig. 4 Orpheus-X4 robot with sensor head and landing area for multicopters

A. Orpheus-X4

The Orpheus-X4 (see Fig. 4) is an experimental reconnaissance robot based on the Orpheus-AC2 model made by our team to facilitate the measurement of chemical and biological contamination or radioactivity for military. The Orpheus-X4 offers the same drive configuration as its predecessor, namely the four extremely precise AC motors with harmonic gears directly mechanically coupled to the wheels; this configuration makes the robot very effective in hard terrain and enables it to achieve the maximum speed of 15 km/h. The main difference lies in the chassis, which is not designed as completely waterproof but consists of a series of aluminum plates mounted on a steel frame of welded L-profiles. This modular structural concept makes the robot markedly more versatile, and this is a very important aspect in a robot made primarily for research activities. Furthermore, the device is equipped with a 3DOF manipulator for the sensor head. The manipulator, again, comprises very powerful AC

motors combined with extremely precise, low backlash harmonic drive gearboxes made by the Spinea company. The presence of such precise gearboxes can be substantiated by several reasons, mainly by the fact that the robot is used not only for telepresence but also for mobile mapping and SLAM. As currently planned, the robot's only proximity sensor is the TOF camera placed on the sensory head. The Orpheus robots are described in more details in our previous papers, such as [9].

B. Sensor Head

The sensor head containing five optical sensing elements is shown in Fig. 5. The sensors are as follows:

• Two identical tricolor CCD cameras (see 1 in Fig. 5): TheImagingSource DFK23G445 with the resolution of 1280x960 pixels, max. refresh rate of 30Hz, and GiGe Ethernet protocol. This device is equipped with a Computar 5mm 1:1.4 lens. The field of view is 40˚(h) x 51°(v).

• Two identical thermal imagers (see 2 in Fig. 5): Flir Tau 640 with the resolution 640x512 pixels, temperature resolution 0.05K and Ethernet output. The field of view is 56˚(h) x 69˚(v).

• One TOF camera (see 3 in Fig. 5): A Mesa Imaging SR4000 with the range of 10m, resolution of 176x144 pixels, and an Ethernet output. The field of view is 56˚(h) x 69˚(v).
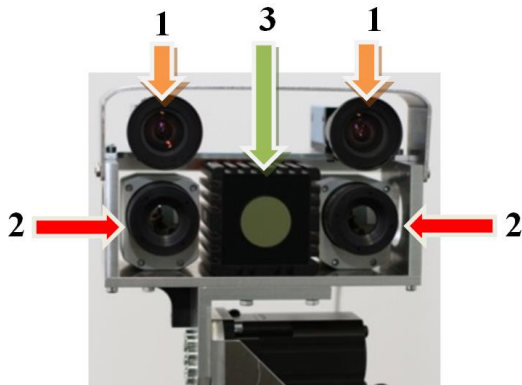

Fig. 5 the sensor head. 1 – tricolor CCD cameras; 2 – thermal imagers; 3 – TOF camera

The largest FOV capture thermal imagers and the TOF camera, which is required for the simultaneous use of stereovision and thermal stereovision. The main disadvantage of the applied TOF camera is its low number of pixels (spatial resolution). Compared to the CCD cameras, it is about 10 times lower in one axis, and in relation to thermal imagers it is 4 times lower.

III. SENSOR HEAD CALIBRATION

Here will be described only calibration of intrinsic and extrinsic parameters. It is also necessary to calibrate temperatures of thermal imagers, in detail described in [11] and TOF camera measured distances, this calibration is described in detail in [12].

First condition for successful calibration is calibration plate with pattern visible in all 3 used spectrums:

• Infrared for TOF camera (850 nm).
• Visible spectrum for CCD cameras.
• Long-wavelength infrared for thermal imagers.

We proposed calibration plate based on checkerboard pattern (see Fig. 6). The plate consists of an aluminum panel (low emissivity, high reflectivity) with a laser-cut, anodized pattern and chipboard covered by a black, matt foil (high emissivity, low reflectivity). Anodizing of aluminum panel reduces high reflectivity. Good contrast of checkerboard pattern for thermal imagers was achieved by active heating of aluminum part at 50°C.
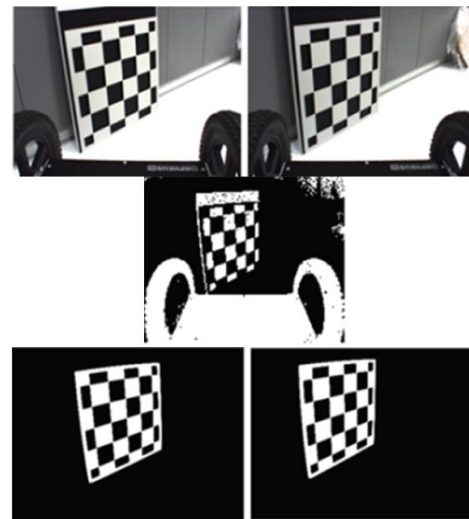

Fig. 6 the final calibration plate: the left and right CCD cameras (up); the TOF camera intensity image (center); the left and right thermal imager cameras (down)

Software MultiSensCalib was created for calibration of intrinsic and extrinsic parameters of sensor head camera system. The calibration comprises the following stages:

• Corner extraction based on automatic corner extraction from Omnidirectional Camera Calibration Toolbox for Matlab [7]. Used algorithm is described in detail in [8]. If automatic corner extraction doesn't converge to solution, manual marking for 4 corner of calibration plate is used. Then corners are refined according to algorithm used in [9].

• Homography from extracted corners.

• Intrinsic and extrinsic parameters are computed from homography according to [4].

• Nonlinear optimization that minimizes the sum of the squares of the re-projection errors including the determination of distortion first for each camera separately and then for all together.

More details about calibration are described in [11].

The authors decided to make the software, including source code, publicly available. The executable, Matlab source code and sample images are available for download at

http://www.ludekzalud.cz/multisenscalib/

IV. DATA FUSION

Data fusion is performed by means of image transformations. The range measurements of the TOF camera can be displayed into images of the CCD cameras and thermal imagers using spatial coordinates. The thermal image can be displayed into the CCD image according to identical points (ID) of the TOF camera transformed into frames of the CCD camera and the thermal imager and vice versa (see Fig. 7).
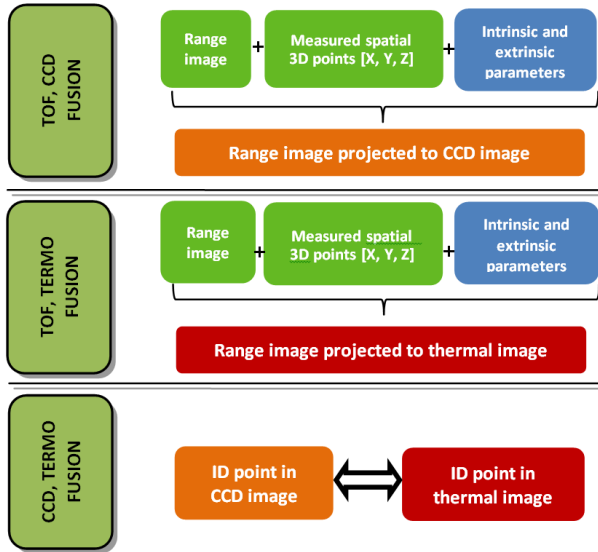

Fig. 7 scheme of data fusion: TOF and CCD data fusion (up); TOF and thermal data fusion (centre); CCD and thermal data fusion (down)

The input data for data fusion include the range measurement, the image coordinates of all sensors, and the results of previous calibration. The procedure comprises the following stages:

• Computation of spatial coordinates measured by TOF camera.

• Homogeneous transformation to determine measured spatial coordinates in frames of other cameras.

• Perspective projection to determine image coordinates in frames of other cameras.

• Correction of recalculated image coordinates to the calibrated position of the principal point.

The spatial coordinates X, Y, and Z are computed according to Eq. (1) and Eq. (4), where x, y are image coordinates of TOF camera, f focal length and d_0 is measured distance projected on optical axis. Calculation of spatial coordinate Z in Eq. (2) is simplified by substitution of cyclometric function Eq. (3).

$$X = \frac{d_0 x}{f}, Y = \frac{d_0 y}{f} \qquad (1)$$

$$Z = d_0 = d \cos\left(\arctan\left(\frac{y}{\sqrt{f^2 + x^2}}\right)\right) \cos\left(\arctan\left(\frac{x}{f}\right)\right) \qquad (2)$$

$$\cos(\tan^{-1} a) = \frac{1}{\sqrt{1 + a^2}} \qquad (3)$$

$$Z = \frac{df}{\sqrt{x^2 + y^2 + f^2}} \qquad (4)$$

The homogeneous transformation is determined by Eq. (5), where $R_{[3\times3]}$ is the rotational matrix, $t_{[3\times1]}$ is the translation vector, and X', Y', Z' are the spatial coordinates of the second sensor. The image coordinates of the TOF camera in the next frame x_c', y_c' are computed using perspective projection Eq. (6), where f' is the focal length of the second sensor.

$$\begin{bmatrix} X' \\ Y' \\ Z' \\ 1 \end{bmatrix} = \begin{bmatrix} R & t \\ 0 & 1 \end{bmatrix} \begin{bmatrix} X \\ Y \\ Z \\ 1 \end{bmatrix} \qquad (5)$$

$$x_c' = \frac{f'X'}{Z'}, y_c' = \frac{f'Y'}{Z'} \qquad (6)$$

V. OPTIMAL IMAGE CONFIGURATION

Selection of appropriate image configuration is a vital part of the whole calibration process and it has great impact to calibration results, and subsequently to multispectral data-fusion quality and robustness. To choose the most appropriate configuration, we started with 10 image configurations, see Table 1. Blue dots in second column denote image in normal position and blue arrows denote direction of image acquisition. 2-9 images were used for sensory head calibration. Edges of images that do not contain calibration target, are greater than usually, because of cameras rotations in sensory head and different fields of view.

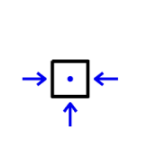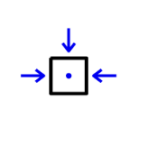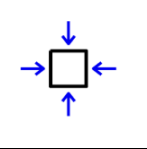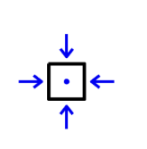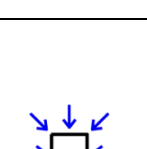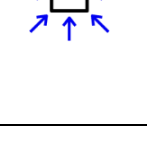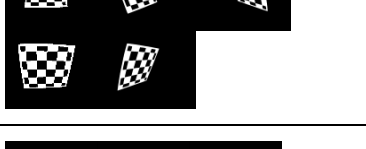| Conf. No.	Scheme of image acquisition	Examples of images for thermal imager
1		
2		
3		
4		

Table 1 investigated image configurations for sensory head calibration

The most effective configuration was determined according to independent evaluation of data fusion precision.

The principle of this evaluation is comparison of identical objects directly extracted from images from CCD cameras and thermal imagers with objects extracted from images from TOF camera and projected to CCD cameras and thermal imagers frames, using data fusion algorithm.

We had to propose objects for this verification that may be easily identifiable in the all corresponding images.

Design of target clearly identifiable in images of all cameras was aluminum circle covered with black paper in the middle and with 3M red reflective tape on the edge with active heating. Reflective tape is used for easier identification of targets in images of TOF camera, but significant disadvantages of this reflectivity is missing measured distances, since too big portion of light is returned unidirectional. The matte paper in

the middle of the circle was used to overcome this problem – it is easy-to-be-identified by the TOF camera. We used 3 aluminum circles with 20 cm and 30 cm diameters. The targets are well identifiable on images of all 3 camera types (see Fig. 8).
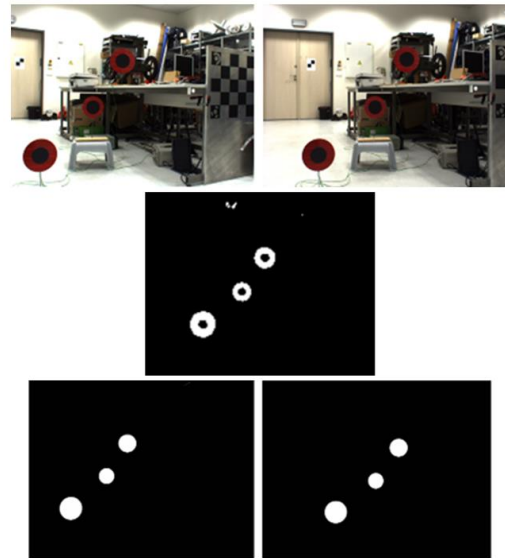

Fig. 8 the images of final target for the verification of the data fusion accuracy: the left and right CCD cameras (up); the TOF camera intensity image (center); the left and right thermal imager cameras (down)

Eighty-seven images were obtained in the experiment under real indoor conditions from the free ride of the robot. 211 extracted objects were used for data fusion evaluation, TOF camera image radial distance for these objects was in range from 1-67 pixels, range for measured distance was from 1.1 to 5.7 m.

Extraction of targets from images comprises the following stages:
• Thresholding.
• Removing small objects (noise) using morphological opening.
• Connection of separated parts using morphological closing.
• Filling closed objects.
• Determining of centroid coordinates.

The most suitable configurations according to values of standard deviations are configuration 8 and 10, but configuration 8 contains error increasing with image radial distance, in detail described in [17]. Configuration 10 of images is reliable according to proposed evaluation of data fusion.

Table 2 shows standard deviations σ_x, σ_y of image coordinates x, y projected by proposed data fusion algorithm for tested configurations 4-10. Standard deviation of image coordinates is denoted as σ. Values of standard deviation are given in pixels of CCD cameras and thermal imagers. Values of intrinsic and extrinsic parameters computed from only 2

images, i.e. configuration 1-3, are far away from real values.

Conf. No		Standard deviation od data fusion [pixel]			
		CCDl	CCDr	TH. l	TH. r
4	σ_x	6.3	6.3	2.2	3.5
	σ_y	5.2	6.0	2.3	2.3
	σ	5.8	6.2	2.3	3.0
5	σ_x	2.8	3.3	1.4	1.5
	σ_y	3.9	3.8	1.6	1.1
	σ	3.4	3.6	1.5	1.3
6	σ_x	2.7	3.1	1.3	1.1
	σ_y	3.3	3.3	1.7	1.1
	σ	3.0	3.2	1.5	1.1
7	σ_x	3.7	3.4	1.3	1.3
	σ_y	3.9	3.7	1.3	1.3
	σ	3.8	3.6	1.3	1.3
8	σ_x	2.0	2.4	1.2	1.1
	σ_y	3.2	3.2	1.5	1
	σ	2.7	2.8	1.4	1.1
9	σ_x	2.9	3.5	1.2	1.1
	σ_y	4.1	4.4	1.4	1.2
	σ	3.6	4.0	1.3	1.2
10	σ_x	2.4	3.0	1.0	1.2
	σ_y	3.2	3.3	1.2	1.1
	σ	2.8	3.2	1.1	1.2

Table 2 standard deviations of image coordinates for configurations 4-10

The differences between the extracted centroid coordinates and those projected from TOF image using data fusion algorithm depending on TOF image radial distances is displayed in Fig. 9-Fig. 16for configuration 10. Due to the fact that the TOF camera has the lowest resolution, the following figures show regions that include errors in TOF image centroid extraction in range -0.5 – +0.5 pixel (delimited by the orange horizontal lines).

The boundaries of TOF camera distance measurement accuracy regions, defined by manufacturer [11], are displayed in the following figures.
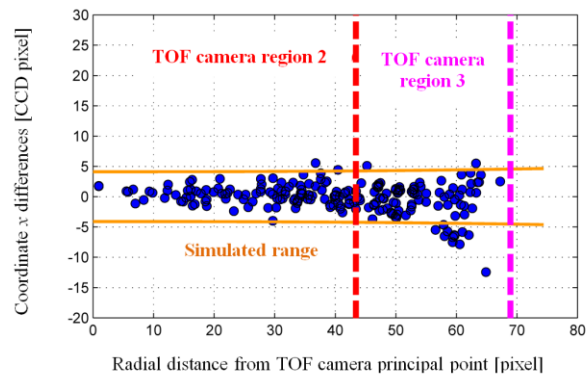

Fig. 9 the coordinate differences determined from the extracted centroids in images of the left CCD camera and from projected TOF image coordinates using the data fusion algorithm: the coordinate x differences
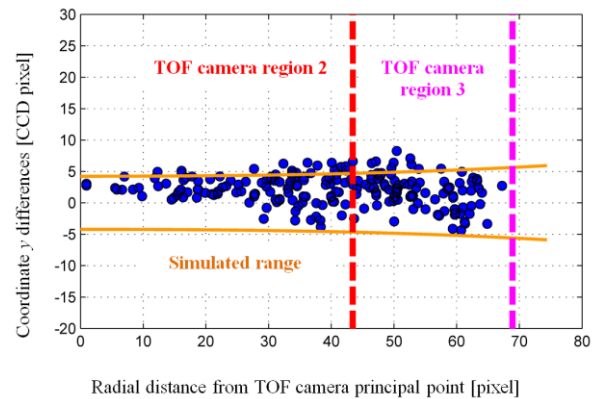

Fig. 10 the coordinate differences determined from the extracted centroids in images of the left CCD camera and from projected TOF image coordinates using the data fusion algorithm: the coordinate y differences
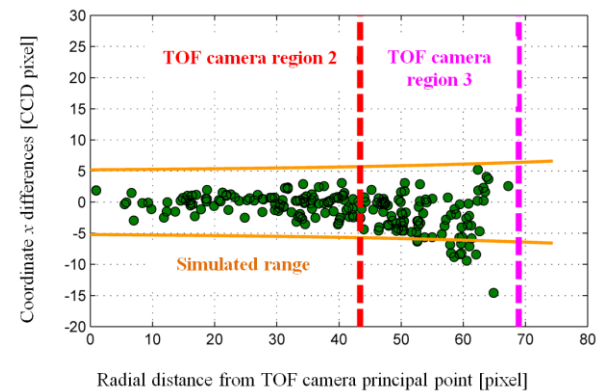

Fig. 11 the coordinate differences determined from the extracted centroids in images of the right CCD camera and from projected TOF image coordinates using the data fusion algorithm: the coordinate x differences
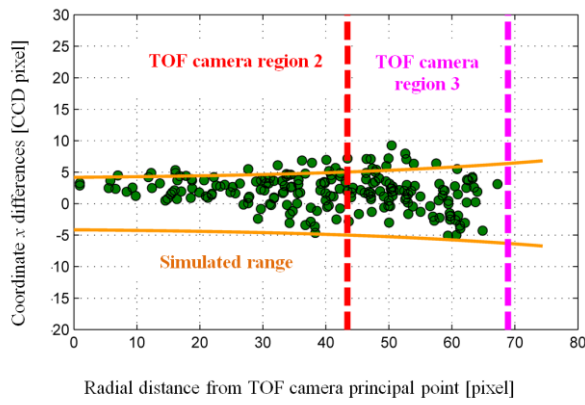
Fig. 12 the coordinate differences determined from the extracted centroids in images of the right CCD camera and from projected TOF image coordinates using the data fusion algorithm: the coordinate y differences
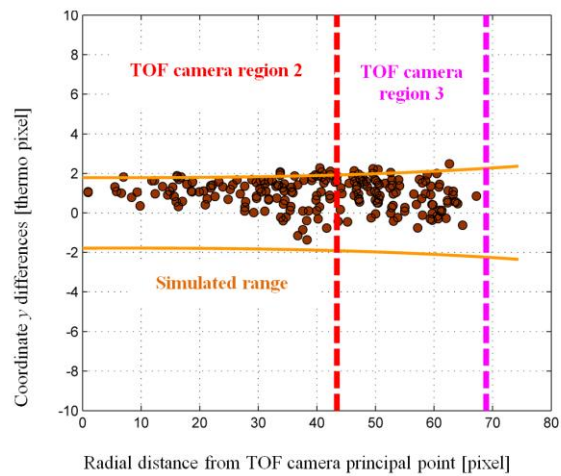

Fig. 14 the coordinate differences determined from the extracted centroids in images of the left thermal imager and from projected TOF image coordinates using the data fusion algorithm: the coordinate y differences

Fig. 13 the coordinate differences determined from the extracted centroids in images of the left thermal imager and from projected TOF image coordinates using the data fusion algorithm: the coordinate x differences
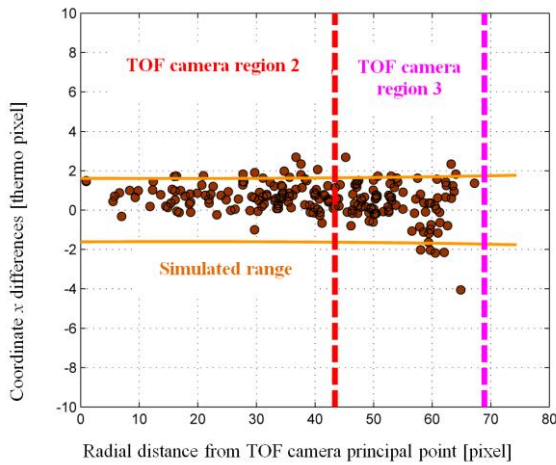

Fig. 15 the coordinate differences determined from the extracted centroids in images of the right thermal imager and from projected TOF image coordinates using the data fusion algorithm: the coordinate x differences
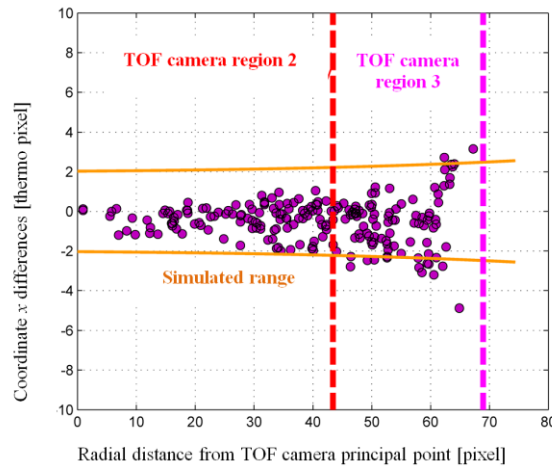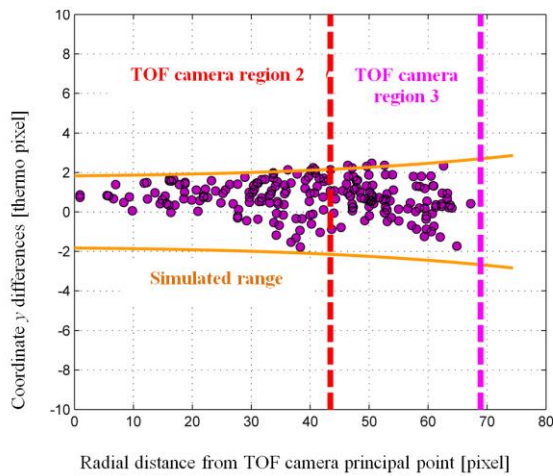
Fig. 16 the coordinate differences determined from the extracted centroids in images of the right thermal imager and from projected TOF image coordinates using the data fusion algorithm: the coordinate y differences

VI. MULTISPECTRAL MAPPING

The data fusion for map building differs from the one used for telepresence in that only one CCD, one thermal imager, and one TOF camera are used. Since the calibration is performed for all the cameras, the unused cameras can be employed equally to the already used ones. At the moment, the unused devices only serve as a backup. In the future, we expect them to be utilized for occlusion detection and correction.

A. Block Division of the Global Map into Cells

Since the mapping system is going to be used in abovementioned reconnaissance robotic system CASSANDRA, the vital requirement of the mapping system is its scalability; this factor should be achieved without any impact on the precision. While outdoor environments may be easily described by leveled maps, indoor environments are better defined by occupancy grids [18]. This leads to differences in the description of indoor and outdoor environments. In reconnaissance missions, however, both eventualities may occur, even together during single mission; it is therefore necessary to use a hybrid map that allows the storage of both types of maps to one heterogeneous structure.

The result of our research consists in a system where the environment is divided into numbered areas with defined and constant edge lengths. Each of the areas can contain none, a single, or more cells stored in independent files. This arrangement ensures the scalability of the system in the case that, during exploration, the map grows in size. If the size of the map area edge is large enough compared to the measurement range of a given robot, it is not necessary to load the whole map in the memory; only certain environments may be processed, which leads to a fundamental reduction of the processed data and a faster response of the system to the measurement.

The system facilitates the storage of more types of data in each block. Although our system allows for the usage of more structures (Feature map, Level map, Occupancy grid and Evidence grid), only Evidence grids will be used in the processes described below. The evidence grid enables us to store more data in each voxel than the classical Occupancy grid; in our case, the data include the temperature, the color, and the obstacle presence probability. Here, the compression can be performed with Octree. For the correct computation of the incremental differences of the map, all of the fusion operations on the map must be commutative.

B. Map Distribution between Several Robots

The map distribution system in CASSANDRA is inspired by the GIT versioning system [19] [20]. The main difference in the philosophy of these systems consists in that only the last version of the map is stored because no map history is required. This significantly reduces the amount of stored data and accelerates data processing.

At the beginning, the map server distributes the initial map to all of the robots. The initial map may be empty or may contain appropriate map data. After a delay, the robots send their measurements to the server. The mapping system automatically determines which robot misses which measurement from the given set. When a robot intends to update his local map to possess all data from the map server, then it requests the map server for the missing measurement set.

This system ensures that all the robots receive all the measurements from the other robots. Generally, the individual measurements may be seen as aggregated map-difference files, identically as the GIT sees aggregated file differences. It is necessary to perform an online calculation of differences between the main map and an older version of the same map; this can be easily achieved by fixing the given map in a different branch of the graph, similarly as the GIT produces repository branches.

We use Octree to transfer the maps between the map server and the robots. It is convenient that, in most cases, the differential maps will contain a considerable amount of empty space, and the compression ratio between the Evidence grid and the Octree will likely be very high; although the compression is principally lossless, the amount of data to be transmitted will be considerably lower.

The difference map calculation requires, as a precondition, an older map version stored in memory, which leads to the necessity of a large memory capacity on the part of both the map server and the robot. As the hardware on the mobile robot is supposed to be rather limited, we may also not use the map differences on the robot; conversely, a substantial increase in the communication payload is assumed.

For these reasons, the system is capable of using both of the above-mentioned approaches. In this context, further description comprises two components, namely basic operational tools for robots with limited memory resources, and an extended version for sufficiently equipped devices.

The entire communication between the robots and the map server is based on a custom extension of the HTTP protocol. Particular map operations are selected via a server request, and the path to the file directly identifies a map or its branch.
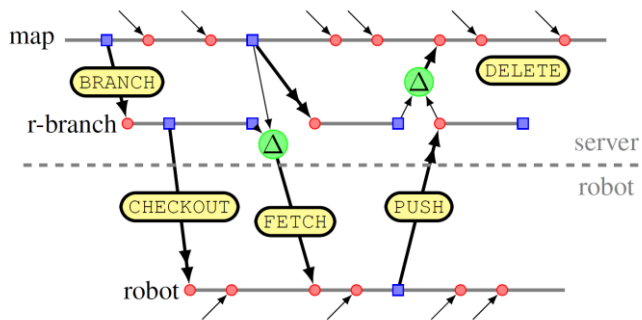

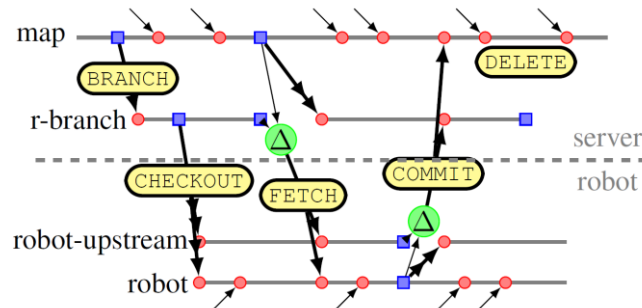Fig. 17 basic operations for map distribution (low-end robots)

Fig. 18 advanced operations for map distribution (hi-end robots)

The activities of the operations are graphically demonstrated in Fig. 17 and Fig. 18. Here, one cycle of robot registration, map transmission, map updating and robot de-registration is presented.

C. Multispectral Mapping Experiment

As a verification experiment, we made multispectral digital maps of our three robotic laboratories connected by a corridor (Fig. 19).

All the data (in the voxel resolutions 2 cm, 4 cm and 8 cm) taken from the same measurement set in the zip-compressed Octree format are available at the webpage http://www.uamt.feec.vutbr.cz/en/projects/multispectral. The primary data is available upon request only since their size exceeds 16GB.

The system comprised 56 cells split equally into two levels. The cell distribution is 2x2x5 cells in the laboratories, 2x2x7 cells in the main corridor, and 2x2x2 cells in the corridor extension (Fig. 18).
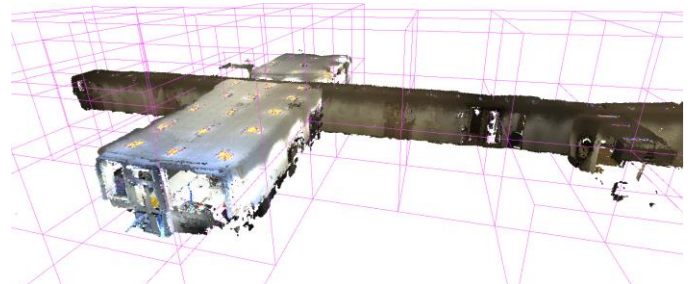

Fig. 19 the interiors measured in the experiment

Fig. 20 A perspective view of the resulting map: the two laboratories (left); the long main corridor; the short extending corridor (far right). The individual cells are represented by the violet lines.

The experiment was performed at night to achieve equal light conditions. We made 54 measurements along two perpendicular paths (26 in the laboratories and 28 in the corridors), with the average spacing of 0.7m (±0.1m) in the laboratories and 1.4m (±0.4m) in the corridors. The spacing distribution was selected unequally depending on the number of objects in the vicinity of the robot. Each measurement comprised 36 individual scans with the movement of the 3DOF manipulator on the Orpheus-X3, where only the upper two degrees of freedom were used. The arm movements were the same during each measurement and were calculated to cover the entire visible environment to be recognized around the robot. The data containing parts of the robot was excluded during the primary filtration.
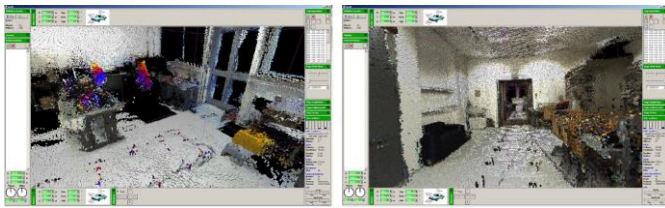
Fig. 21 the indoor mapping experiment – demonstration screenshots of the resulting map
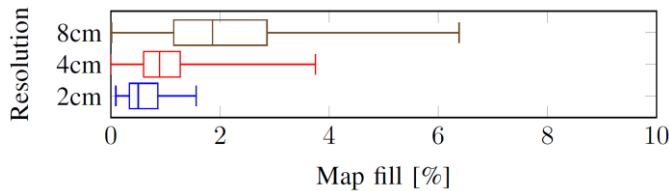

Fig. 22 the map filling dependence on the map resolution with the same primary data

It is obvious from the measurements that the filled area increases with decreasing map resolution. The acquired points are larger and thus occupy a larger volume; this is clearly visible in the boxed-plot graph shown in Fig. 22.
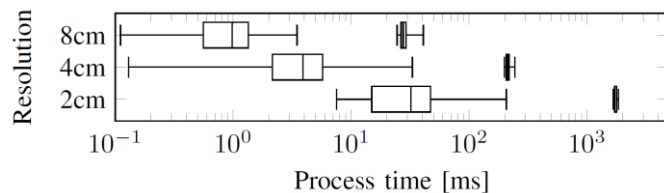

Fig. 23 the time needed for the Octree-Evidence Grid map conversion depending on the resolution. The left graph corresponds to Octree store, and the right graph corresponds to reading from Octree; statistics are made from all the data

We also performed statistics of the Octree map compression and decompression; these results are visible in the above graph (Fig. 23). This graph indicates that the time required by the compression is about an order higher than the time necessary for the decompression. This is caused by the algorithm itself: for the compression, we need to go through and test all the points, while only the occupied points are touched in the decompression.

The final statistics are shown in Table 3. These statistics utilize all measurement data from two map resolutions.

Value	Resolution 4cm	Resolution 2cm
Uncompressed cube [MB]	16	128
Compressed cube (avg.)[MB]	0.081	0.544
Uncompressed map [MB]	640	5120

Compressed map [MB]	8.5	27.7
Compression ratio [-]	1:75	1:185

Table 3 evidence grids vs. octree - compression statisctics

VII. CONCLUSION

As it is apparent from evaluation experiment described in Chapter 5, the multispectral sensor head calibration described in Chapter 3 and fusion (see Fig.24) described in chapter 4 is possible, but has its limits. The main problems come from the fact, the cameras used in the described case have significantly different spatial pixel resolution. It has to be said, the cameras were carefully selected to have parameters appropriate for Orpheus-X4 robot's main mission – real-time telepresence with augmented reality containing thermal information. The cameras had to be small, lightweight, but they had also offer unusually wide field-of-view, since the main operation mode is telepresence with operator wearing head-mounted display. For bigger robots we can suppose that sensors with considerably higher resolution might be used. We can also with high confidence suppose the sensor resolution will increase considerably in time – mainly thermal cameras and 3D proximity cameras.

Numerical evaluation of data fusion algorithm is as follows: standard deviation for x, y image coordinates is around 3 pixels for CCD cameras (0.3 pixel of TOF camera) and around 1 pixel for thermal imagers (around 0.5 TOF camera pixels).

The presented calibration process and evaluation may be used for visual and optical measurement systems of mobile robots in general, so its use is much wider than on presented Orpheus-X4 robot demonstrator.

Fig. 24 image of CCD camera (upper left), image of thermal imager (upper right), uncalibrated data fusion (bottom left), calibrated data fusion (bottom right)

To make the calibration fast and user friendly, we developed application MultiSensCalib in Matlab, which is available both in executable and source code in http://www.ludekzalud.cz/multisenscalib/ The same webpage also contains a set of testing images from Orpheus-X4's sensory head and brief description of the software usage.

Acording to the mapping algorithms, the methods presented in this paper are sufficiently applicable, stable, and reliable, but our research on the telepresence and mapping subsystem of CASSANDRA is still far from complete. The system proved to work sufficiently well in indoor conditions. The described technique of environment division into spatial areas with predefined size, together with their "lossless compression" through octree and synchronization through described GIT-like system proved to be appropriate even for today's wireless communication systems as wi-fi.

The challenge we are currently facing is to facilitate seamless combination of visual telepresence and digital maps to form an augmented reality system. The system should be able to add map information to the real-time telepresence image so that the operator could see data such as the temperatures through a robot that not equipped with a thermal imager; furthermore, it should also facilitate the vision through or behind objects. At present, we are able to achieve this goal with limited features for the stationary robot; however, the exploration experience is outstanding even under the given conditions. For further reference, it is possible to access the real-time demonstration video at http://www.uamt.feec.vutbr.cz/en/projects/multispectral.

REFERENCES

[1] T. Luhmann, J. OHM, J Piechel and T. Roelfs, "Geometric Calibration of Thermographic Cameras", in International Archives of Photogrammetry, Remote Sensing and Spatial Information Sciences 2010, vol. XXXVIII, pp. 411-416

[2] X. Ju, J.-C. Nebel, J. P. Siebert, H. Gong, Y. Cai and J.-P. Chatard, "3D thermography imaging standardization technique for inflammation diagnosis", in Proceedings of the SPIE . 2005, vol. 5640, pp. 266-273

[3] S. Prakash, P. Y. Lee and T. Caelli, "3D Mapping of Surface Temperature Using Thermal Stereo", in 9th International Conference on Control, Automation, Robotics and Vision IEEE, 2006, pp. 1-4

[4] Z. Zhang, "Flexible camera calibration by viewing a plane from unknown orientations", in Proceedings of the Seventh IEEE International Conference on Computer Vision. 1999. DOI: 10.1109/iccv.1999.791289.

[5] PhotoModeler Pro 5 help. Eos System Inc.: 210 - 1847 West Broadway, Vancouver BC V6J 1Y6, Canada.

[6] J.-Y. Bouguet," Complete Camera Calibration Toolbox for Matlab" [online] http://www.vision.caltech.edu/bouguetj/calib_doc/

[7] D. Scaramuzza,"OCamCalib: Omnidirectional Camera Calibration Toolbox for Matlab" [online]. https://sites.google.com/site/scarabotix/ocamcalib-toolbox

[8] M. Rufti, D Scaramuzza and R. Siewart, "Automatic detection of checkerboards on blurred and distorted images", in 2008 IEEE/RSJ International Conference on Intelligent Robots and Systems. IEEE, 2008, s. 3121-3126. ISBN 978-1-4244-2057-5.

[9] D. C. Herrera, J. Kannala and J. Heikkila, "Joint Depth and Color Camera Calibration with Distortion Correction", in IEEE Transactions on Pattern Analysis and Machine Intelligence. 2012, pp. 2058-2064. ISSN 0162-8828.

[10] L. Zalud, F. Burian, L. Kopecny, and P. Kocmanova, "Remote Robotic Exploration of Contaminated and Dangerous Areas", in International Conference on Military Technologies, pp 525-532, Brno, Czech Republic, ISBN 978-80-7231-917-6, 2013.

[11] L. Zalud and P. Kocmanova, "Fusion of thermal imaging and CCD camera-based data for stereovision visual telepresence", in 2013 IEEE International Symposium on Safety, Security, and Rescue Robotics (SSRR). Linkoping: IEEE, 2013, pp. 1-6. DOI: 10.1109/SSRR.2013.6719344. ISBN 978-1-4799-0880-6

[12] P. Kocmanova, A. Chromy, L. Zalud, "3D Proximity Laser Scanner Calibration", in 2013 18TH INTERNATIONAL CONFERENCE ON METHODS AND MODELS IN AUTOMATION AND ROBOTICS (MMAR), pp 742-747, ISBN 978-1-4673-5508-7

[13] SR4000 Data Sheet, MESA Imaging AG. Rev. 5.1, 2011.

[14] L. Nejdl, J. Kudr, K. Cihalova, et. al. "Remote-controlled robotic platform ORPHEUS as a new tool for detection of bacteria in the environment", in ELECTROPHORESIS, Volume: 35 Issue: 16 , Special Issue: SI, Pages: 2333-2345, 10.1002/elps.201300576

[15] L. Zalud, L. Kopecny, F. Burian, "Robotic Systems for Special Reconnaissance", International Conference on Military Technologies, pp 531-540, Brno, Czech Republic, ISBN 978-80-7231-649-6, Oprox, 2009

[16] F. Burian, P. Kocmanova and L. Zalud, "Robot Mapping with Range camera, CCD Cameras and Thermal Imagers", in 19th International Conference on Methods and Models in Automation and Robotics (MMAR). Miedzyzdroje, POLAND: 2014, pp. 200-205

[17] P. Kocmanova, "Sensor Calibration for Multispectral Data Fusion in Mobile Robotics". Brno, 2015. Ph.D. thesis. Brno University of Technology

[18] A. Elfes, "Using occupancy grids for mobile robot perception and navigation," IEEE Computer, vol. 22, no. 6, pp. 46–57, Jun. 1989.

[19] (2014) Git distributed version control system. [Online]. Available: http://git-scm.com/

[20] S. Chacon, Pro Git, 1st ed. Berkely, CA, USA: Apress, 2009.